

An in-house developed annular bright field detection system

Leonardo Lari¹, Ian Wright, Daniel Pingstone, Jonathan Steward, Daniel Gilks and Vlado K Lazarov

Department of Physics, The University of York, Heslington, YO10 5DD, York, UK
and

The York-JEOL Nanocentre, York Science Park, Heslington, YO10 5BR, York, UK

E-mail: leonardo.lari@york.ac.uk

Abstract. Annular bright field (ABF) detectors have been developed in the last few years allowing the direct imaging of low-Z atoms from oxygen down to hydrogen. These types of detectors are now available as standard attachments for the latest generation of top-end electron microscopes. However these systems cannot always be installed in previous generation microscopes. In this paper we report the preliminary results of an in-house implementation of a ABF detection system on a CEOS aberration corrected JEOL 2200FS STEM. This has been obtained by exploiting the standard BF detector coupled with a high vacuum compatible, X-ray tight and retractable shadowing mechanism. This results in the acquisition of near zero-angle scattered electrons with inner collection semi-angle from 2.0 mrad to 23 mrad and outer semi-angle in the range from 3.0 mrad to 35 mrad. The characteristics and performances of this ABF detection system are discussed.

1. Introduction

In the last decade, probe aberration corrected scanning transmission electron microscopy (STEM) has proven to be one of the leading methods for atomic scale investigation of crystalline materials. The advantage of these methods lies mostly in the high angle annular dark field (HAADF) imaging which features the so-called Z-contrast, where the intensity of the image is proportionally related to the power of two of the atomic number. This property makes HAADF images readily interpretable without the need of extensive image simulations [1]. One of the deficiencies of the HAADF imaging is inability to image light elements, e.g. oxygen and other low Z elements, due to their low electron scattering power. Recently, annular bright field (ABF) detectors have been developed allowing direct imaging of low-Z atoms, as oxygen in strontium titanate [2]. Starting initially by using bright field detectors in conjunction with a beam stopper [3] ABF detectors are now available as standard attachments for the latest generation of top-end electron microscopes, and have been demonstrated to be able to directly image lithium columns in LiV_2O_4 using a JEOL R005 [4] and more recently hydrogen columns in VH_2 using a JEOL ARM microscope [5]. However, these systems with a dedicated detector cannot always be installed in previous generation microscopes. In this work we present preliminary results obtained by an ABF detection system in-house designed and developed which can provide a relatively cheap solution for implementing an ABF detector on earlier generation STEM equipped with a BF detector.

¹ To whom any correspondence should be addressed.



2. Methods

A beam shadowing mechanism was designed to block the central part of the standard JEOL bright field (BF) STEM detector of a JEOL 2200FS double CEOSTM aberration corrected (S)TEM operating at 200kV and equipped with an in-column Omega type electron energy filter. Figure 1a) shows its

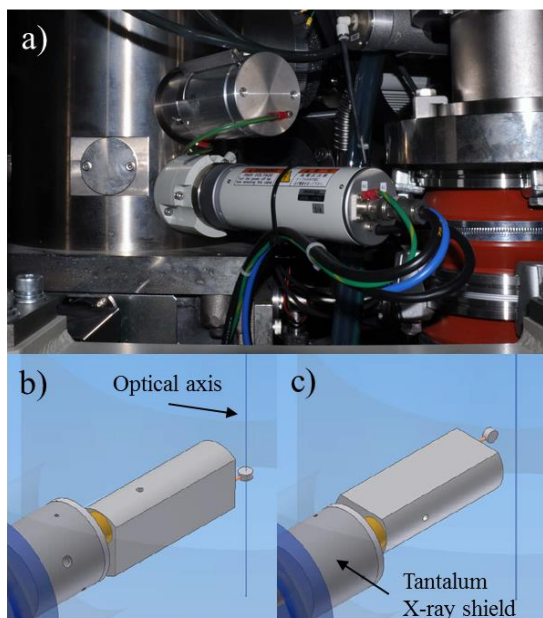


Figure 1. a) location of the ABF beam stopper above the bright field detector in the camera chamber; b) beam stopper *ON* position; c) beam stopper *OFF* position

testing its performance. Si [110] and SrTiO₃ [110] crystals were mechanically polished and ion milled to electron transparency using the cross sectioning methodology as described in [6].

location in the port above the BF detector located in the camera chamber of the microscope. This port is normally used to place a post omega filter annular dark field detector. The beam stopper (BS) was made in the departmental workshop using Al for the parts to go inside the camera chamber, and steel to interface the beam stopper to the microscope column. An Al rod holds an off-axis beam stopping disk. The rod rotates around its axis and has two rest positions one centred on the electron optics axis (*ON* position, Figure 1b) and at 90 degrees (*OFF* position, Figure 1c) where is retracted out of the electron beam path. The BS disk has a diameter of about half of the size of the BF detector entrance aperture. An additional mechanism was fitted to allow fine centring of the BS respect to the BF detector axis. Protection from X-ray generated by the beam stop is provided by a cylinder of Ta mounted around the Al rod at the internal side of the camera chamber wall as indicated in Figure 1c). X-ray leakage trough the chamber was tested using a Thermo ScientificTM Mini 900X radiation monitor.

Two TEM samples were prepared for measuring the ABF detector acceptance semi-angles and for

3. Results and discussion

The response of the BF detector as a position of the electron beam is shown in Figure 2a). The electron beam was allowed to scan an area encompassing the BF detector entrance aperture in STEM alignment mode. A scanning time of 19msec and the smaller condenser aperture (12mrad convergence

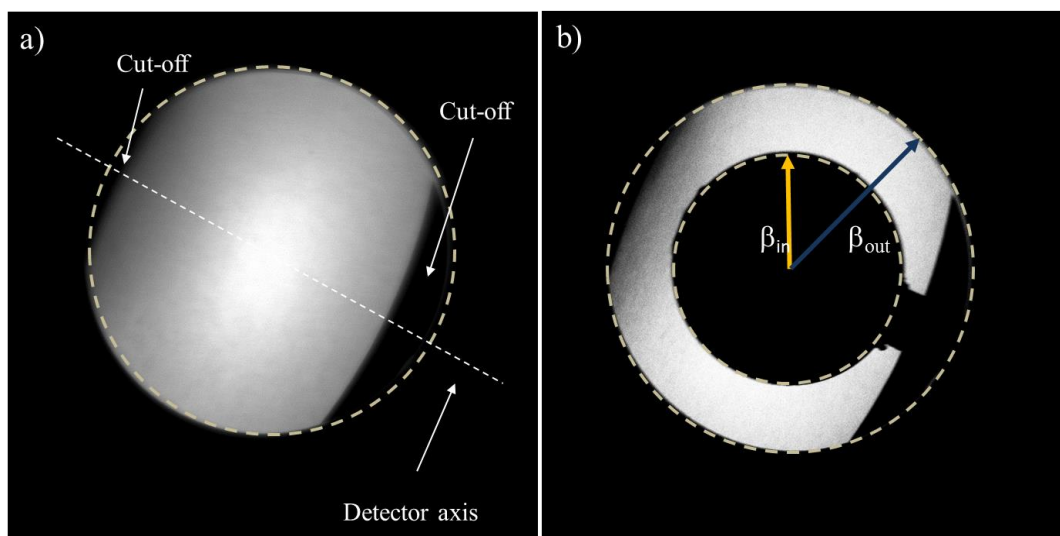


Figure 2. a) Large field of view BF STEM image showing the BF detector response; b) BF detector configuration showing inner and outer collection semi-angles.

semi-angle) was used in order to avoid saturation of the BF detector. During the image acquisition the beam stopper was kept in the *OFF* position. As indicated by the two arrows inset in Figure 2a) there are two cut-off areas perpendicular to the detector axis. Figure 2b) shows the ABF configuration with the beam stopper centred respect to the BF detector. Using the Si [110] sample the inner collection semi-angle β_{in} and the outer one β_{out} were measured from Kikuchi lines spacing for each of the fifteen camera length setting available in STEM mode for our microscope. The results are listed in Table 1. Larger camera length values produce very narrow collection ranges contained within the central region of the BF detector hence the imaging is coherent and very close to normal BF conditions.

Table 1. List of ABF acceptance semi-angles versus nominal camera length settings

Camera length	β_{in} (mrad)	β_{out} (mrad)
4 cm	23.4	38.7
5 cm	20.0	33.0
6 cm	16.6	27.3
8 cm	11.1	18.3
10 cm	9.5	15.6
12 cm	7.8	12.8
15 cm	7.0	11.6
20 cm	6.2	10.3
25 cm	6.1	10.1
30 cm	7.7	12.7
40 cm	6.3	10.4
50 cm	5.2	8.6
60 cm	5.0	8.3
80 cm	4.5	7.4
100 cm	3.1	5.1
120 cm	2.5	4.1
150 cm	2.0	3.2
β_{in} inner semi-angle; β_{out} outer semi-angle		

However, shorter camera lengths (from 4 cm to 10 cm) enable larger shadowing of the central part of the BF detector (above 10 mrad) which provides angular acceptance range close to the standard ABF values as used in [5]. Figure 3 a) shows a HAADF image of the SrTiO₃ sample acquired along the [110] zone axis. In this projection three distinctive atomic columns are present, O and Ti single columns and Sr/O mixed column. The HAADF image was acquired in the range 85-170 mrad. Brighter columns correspond to the columns occupied by Sr atoms. Scanning instabilities are visible as streaks running at about 45 degrees with respect to the horizontal. In the same acquisition conditions (50 cm camera length) an ABF image was acquired as shown in Figure 3b). Probe deconvolution using a maximum entropy approach [7] was applied to the collected HAADF images as shown in Figure 3, whereas the ABF image (Figure 3b) was filtered using the smooth function of GatanTM Digital Micrograph.

A full series of simulations of SrTiO₃[110] were produced using QSTEM [8] for the range of camera length settings available. The aberration coefficients obtained by the CEOSTM stem alignment software at the beginning of the microscopy session were used as calculation parameters, nominally tri-fold astigmatism 22nm, axial coma 15nm, spherical aberration coefficient 1.1 μ m, four-fold astigmatism 660nm, star aberration 316 nm, and five-fold astigmatism 80 μ m. The multislice simulations were performed using the frozen phonons approximation. The best fit for the acceptance semi-angle used 5.2-8.6 mrad was obtained for a sample thickness of 360 slices corresponding to 99 nm, as shown in the inset of Figure 3b). Deviation from a perfect match with the experimental image can be due, besides the noise, to the portion of the signal cut off as

shown in Figure 2. On the left side there is a reduction of the outer collection semi-angle of about 15% while on the other side (without considering the rod where the blanker is attached) the reduction is of 25%. Nevertheless this problem could be solved by introducing an annular aperture instead of a central beam stopper. This would practically imply the use of the lower camera length settings.

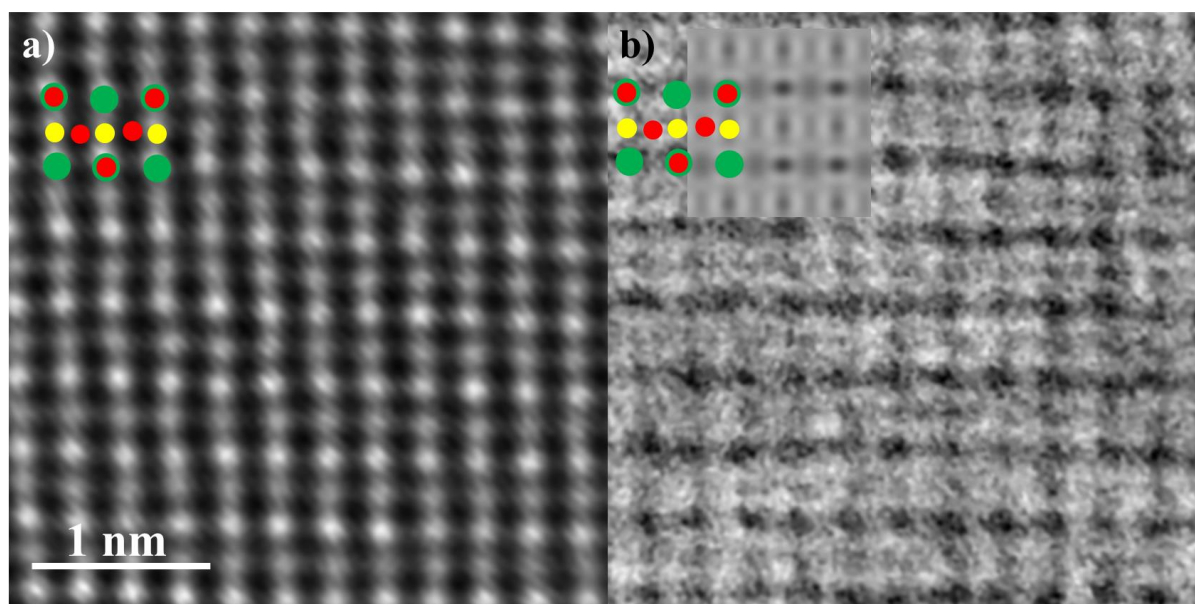


Figure 3. a) HAADF STEM image of SrTiO₃ along [110] zone axis; b) ABF image from same area as in a) with collection semi-angles ($\beta_i=5.2$ mrad and $\beta_o=8.6$ mrad). Atoms are colour coded as following: yellow (Ti), green (Sr) and red (O).

4. Conclusions

In this paper we have shown the preliminary results of an in-house developed annular bright field detection system using a beam stopper coupled with the existing standard STEM bright field detector. The bright field detector collection area was found to be irregular with a reduction of collection semi-angle along the detector longitudinal axis of 15% and 25% respectively on each side. Useful camera lengths setting for appropriate shadowing of the central bright field region was found only for nominal camera lengths below 10cm. Our findings indicate that an annular aperture coupled with the bright field detector, instead of a beam stopper, would better define the ABF collection semi-angles to be fed into the image simulation software.

Acknowledgments

The authors would like to thank the University of York Physics department workshop technicians for their help with this project.

References

- [1] Nellist P D and Pennycook S J 2000 *Advances in Imaging and electron physics* **113** 147
- [2] Okunishi E, Ishikawa I, Sawada H, Hosokawa F, Hori M, and Kondo Y 2009 *Microsc. Microanal.* **15** 164–165
- [3] Findlay S.D., Shibata N, Sawada H, Okunishi E, Kondo Y and Ikuhara Y 2010 *Ultramicroscopy* **110** 903–923
- [4] Oshima Y, Sawada H, Hosokawa F, Okunishi E, Kaneyama T, Kondo Y, Niitaka S, Takagi H, Tanishiro Y and Takayanagi K 2010 *Journal of Electron Microscopy* **59** 457–461
- [5] Findlay S D, Saito T, Shibata N, Sato Y, Matsuda J, Asano K, Akiba E, Hirayama T and Ikuhara Y 2010 *Applied Physics Express* **3** 116603
- [6] Lari L, Lea S, Feeser C, Wessels B W, and Lazarov V K. 2012 *J. Appl. Physics* **111** 07C311
- [7] Grillo V. 2011 *Microscopy and Microanalysis* **17** 1292
- [8] Koch C T, “Determination of core structure periodicity and point defect density along dislocations”, PhD thesis, Arizona State University (2002)